RSC Advances

PAPER

View Article Online
View Journal | View Issue



Cite this: *RSC Adv.*, 2024, **14**, 27354

# Characterization of the daucosterol–lecithin complex and its impact on lipid metabolism in hyperlipidemic mice

Yipeng Gu, [a] Liang Shuai,[b] Dingjin Li,[a] Mobo Song,[a] Yingjian Liu[a] and Xiaomei Yang*[a]

Received 11th May 2024
Accepted 19th August 2024

DOI: 10.1039/d4ra03471f

rsc.li/rsc-advances

This investigation delves into the daucosterol–lecithin complex (DS–LC) and its effects on lipid homeostasis in hyperlipidemic mice. DS–LC was assessed for complexation efficiency, physicochemical properties (UV, XRD, FTIR, SEM, DSC), and its impact on organ health and serum lipid levels. The results revealed that daucosterol formed an effective complex with lecithin at a 2 : 1 ratio, producing a translucent beige DS–LC with distinctive aggregation. UV-vis spectra confirmed that daucosterol's chromophore structure remained intact in DS–LC, indicating no new compound formation. FTIR analysis identified hydrogen bonding and increased molecular association without changing lecithin peaks, highlighting specific intermolecular interactions. SEM and XRD showed that complexation transformed daucosterol into an irregular form within the lecithin matrix, forming a new phase and demonstrating a strong lecithin–daucosterol interaction. Thermal analysis suggested homogeneous daucosterol distribution due to intermolecular interactions. DS–LC treatment effectively alleviated hyperlipidemia, enhancing liver function and reducing lipid accumulation in epididymal fat. It also significantly decreased total cholesterol, triglycerides, LDL-C, and arteriosclerosis index in hyperlipidemic mice, indicating DS–LC's potential as a therapeutic agent for lipid metabolism and related metabolic disorders.



## 1 Introduction

Hyperlipidemia, an ancient yet increasingly prevalent disorder, manifests as elevated levels of lipids in the bloodstream.[1–3] These lipids, notably cholesterol and triglycerides, play pivotal roles in physiological processes but pose health risks when present in excessive quantities.[4,5] The accumulation of excess lipids results in the formation of atherosclerotic plaques in arterial walls, thereby causing arterial narrowing and impaired blood flow.[6] Consequently, hyperlipidemia is a significant risk factor for cardiovascular ailments, encompassing myocardial infarction and stroke, while also being associated with conditions like obesity, diabetes mellitus, and hypertension.[4,7] The surge in hyperlipidemia's prevalence in recent decades can be attributed primarily to shifts in lifestyle and dietary patterns.[8] Sedentary behaviors, consumption of high-fat diets, and excessive alcohol intake are among the key contributors.[9,10] These environmental factors interact with genetic predispositions, exacerbating the condition's impact and fostering its widespread occurrence.[11] Maintaining lipid homeostasis is essential for overall metabolic health. To address this challenging issue, numerous efforts have been made to screen potential drugs from bioactive natural ingredients.

Daucosterol, a natural saponin, is essentially a glucoside of β-sitosterol, predominantly synthesized by plants.[12] Derived from the peel of the Chinese plant *Eleocharis dulcis*, daucosterol has shown promise in enhancing insulin sensitivity in type 2 diabetic mice fed a high-fat and high-sugar diet, achieved through the modulation of intestinal flora.[13] Additionally, Jain *et al.*[14] successfully extracted daucosterol from the ethanolic extract of Ipomoea digitata root, demonstrating its hypolipidemic effects by reducing serum total cholesterol and LDL-cholesterol levels. In an *in vivo* study, daucosterol treatment showed significant efficacy in animals with hypercholesterolemia, leading to a remarkable reduction in β-lipoproteins by 46% and blood cholesterol by 31%.[15] However, as a saponin, daucosterol faces challenges due to its large molecular size and poor lipid solubility, resulting in limits its bioavailability within the body. To overcome these limitations, exploring strategies such as phospholipid modification to enhance its solubility, bioavailability, and overall therapeutic efficacy represents one of the effective approaches.

Phospholipid complexes arise through the establishment of non-covalent interactions, including electrostatic attraction, van der Waals forces, and hydrogen bonding, between phospholipids and active substances.[16] These complexes exhibit amphiphilic properties, enhancing their capacity for absorption

[a]*Guangxi Key Laboratory of Health Care Food Science and Technology, Institute of Food Science and Technology, Hezhou University, Hezhou 542899, China. E-mail: yangxiaomei0801@126.com*

[b]*School of Chemistry and Food Science, Nanchang Normal University, Nanchang, Jiangxi 330023, China*

*via* both amphiphilic cell membranes and the lymphatic system, thus boosting the bioavailability of the components. Additionally, phospholipid complexes have the ability to boost drug stability, prolong the duration of action of the components, and delay their elimination.[17] In recent years, these complexes have gained significant popularity in augmenting the oral bioavailability of drugs that are poorly soluble in water. Their utilization presents promising avenues for enhancing drug delivery and efficacy, particularly in formulations targeting lipid metabolism and cardiovascular health.

This research marks the first characterization of the daucosterol–lecithin complex (DS–LC), obtained from the combination of daucosterol extracted from *Eleocharis dulcis* peel and lecithin. Its impact on lipid homeostasis in mice was explored, shedding light on potential therapeutic applications. The complexation efficiency, physical properties, and chemical interactions of DS–LC were assessed. Additionally, the effects of DS–LC on serum lipid levels, organ indices, and histological changes in hyperlipidemic mice were evaluated. Specifically, phospholipid complexes like DS–LC have the potential to optimize the therapeutic efficacy of daucosterol. This is particularly promising in the field of lipid metabolism management and cardiovascular health promotion, offering new possibilities for the future applications of daucosterol extracted from *Eleocharis dulcis* peel.

## 2 Materials and methods

### 2.1 Materials and chemicals

Fresh *Eleocharis dulcis* sourced from the central agricultural product market of Hezhou in China, underwent peel cleaning, drying in a DHG-9140A oven (Keelrein, China), and crushing with a DFY-600 grinder (Linda Machinery Co., Ltd, China). Lecithin was purchased from Shanghai RHAWN Chemical Reagent Co., Ltd, (Shanghai, China). Methanol, tetrahydrofuran, chloroform, ethyl acetate, hexane and dimethyl sulfoxide were obtained from Guanghua Sci-Tech Co., Ltd (Guangzhou, China). All chemical reagents were of analytical grade. Chromatographically pure methanol and distilled water were obtained from Merck Ltd (Darmstadt, Germany).

### 2.2 Preparation of daucosterol–lecithin complex (DS–LC)

Daucosterol was isolated from *Eleocharis dulcis* peel using a modified version of a previous method.[18] The process involved extracting the powdered peel twice with ethanol at a 1 : 5 ratio, combined with ultrasonic extraction at 60 °C and 40 kHz. The filtrates were concentrated to retrieve ethanol and adsorbed onto a silica gel column after mixing with silica gel, and washed with petroleum ether-ethyl acetate until colorless. Ethyl acetate elution isolated the saponin fraction, concentrated, dissolved in hot ethanol, filtered, and recrystallized twice. Further purification was carried out using preparative liquid chromatography with methanol as the eluent and a Developsil ODS HG-5 column under isocratic conditions, yielding daucosterol with a retention time of 61 min. Subsequently, daucosterol and lecithin were mixed at a specific mass ratio and dissolved in tetrahydrofuran. The mixture was magnetically stirred at 40 °C for 2 h. After the tetrahydrofuran was evaporated, trichloromethane was added to dissolve the complexes. Centrifugation at 1000 rpm for 10 minutes resulted in a supernatant containing phospholipid complexes and a precipitate comprising unbound daucosterol. The dried daucosterol–lecithin complexes (DS–LC) were obtained by evaporating the supernatant.

### 2.3 Formation rate of DS–LC rate calculation

The DS–LC was prepared by combining specific quantities of lecithin and daucosterol ($W_1$) at mass ratios of 1 : 1, 2 : 1, and 3 : 1. To quantify unbound daucosterol post-phospholipid complex formation, a standard curve method was employed. Daucosterol standard stock solution, initially prepared at 1 mg mL$^{-1}$ concentration in dimethyl sulfoxide, was diluted to generate standard solutions ranging from 1 mg mL$^{-1}$ to 0.03125 mg mL$^{-1}$. These solutions were analyzed *via* HPLC using a ZORBAX Extend-C18 column with a 100% methanol mobile phase at 210 nm. Analysis was performed at a flow rate of 1 mL min$^{-1}$, 35 °C temperature, and an injection volume of 5 μL. The linear relationship between daucosterol concentration and peak areas (*y*-axis) was established against concentrations of daucosterol standard solutions (*x*-axis), allowing determination of unbound daucosterol weight ($W_2$) in the precipitate. DS–LC formation rate (DFR) was calculated using the following formula.

$$\mathrm{DFR}(\%) = \frac{W_1 - W_2}{W_2} \times 100 \quad (1)$$

### 2.4 Ultraviolet-visible (UV-vis) spectroscopy detection

The daucosterol and DS–LC samples were accurately weighed and then individually dissolved in methanol to achieve a concentration of 1 mg mL$^{-1}$. Methanol was employed as a blank solution to calibrate and zero the spectrophotometer. UV-vis spectroscopy scans ranging from 190 nm to 850 nm were conducted after calibration using the methanol blank. Subsequently, UV-vis spectral scanning was performed on the samples. The UV-vis spectra of each sample were recorded within the designated wavelength range using 10 mm path length quartz cuvettes to ensure precise measurements. The absorption peaks were then analyzed, and the maximum absorption wavelength was recorded.

### 2.5 Fourier transform infrared (FTIR) spectroscopy detection

The FTIR spectroscopy analysis was conducted on sample using the Spectrum Two™ IR spectrometer (PerkinElmer Inc., USA). The KBr pellet method was utilized for sample preparation. Prior to analysis, background correction was performed on each sample, followed by placement on the sample cell. Stable pressure was achieved by adjusting the force gauge for precise spectral scanning. The spectrometer scanned the samples over the wavenumber range of 400–4000 cm$^{-1}$.

### 2.6 X-ray diffraction (XRD) detection

X-ray diffractometry was performed using a D8 Advance X-ray diffractometer (Bruker Corporation, USA) to analyze moderate

quantities of samples. Monochromatic Cu Kα radiation with a wavelength of 1.54056 Å was generated for the experiment. The tube voltage and current were set at 40 kV and 40 mA, respectively. The scanning regions of the diffraction angle ($2\theta$) were adjusted between 5 °C and 80 °C, with a scanning speed of 5 °C $min^{-1}$.

### 2.7 Scanning electron microscopy (SEM)

The testing samples were carefully adhered to a copper testing stub using a conductive adhesive. Subsequently, a thin and uniform layer of gold was sputtered onto the surface of the samples using a sputter coater. The experimental conditions were set at 10 kV and low vacuum to ensure optimal imaging quality and sample stability during observation. The microstructure and surface morphology of the samples were then examined using a scanning electron microscope (JSM-7900F, JEOL Ltd, Japan), allowing for detailed visualization and analysis of their structural characteristics.

### 2.8 Differential scanning calorimetry (DSC)

Differential scanning calorimetry analysis was performed using a DSC Q2500 instrument (TA Instruments, USA) under a nitrogen atmosphere. Samples weighing 5 mg were precisely measured and sealed in aluminum pans with crimped lids to maintain sample integrity during analysis. The thermal cycle was conducted with a heating rate of 10 °C $min^{-1}$, over a temperature range of 20 °C to 350 °C. A nitrogen flow rate of 0.2 mL $min^{-1}$ was maintained throughout the experiment to ensure a consistent environment within the DSC chamber.

### 2.9 Animal grouping and treatment

Male ICR mice, aged 4 weeks, were housed in stainless steel cages under controlled conditions (24 ± 1 °C, 50 ± 10% humidity, and a 12 h light–dark cycle) and provided with water and standard chow ad libitum. After a one-week acclimation period, the mice were randomly assigned to four groups: CON (normal control), MC (model control), LDT (low-dose DS–LC, 100 mg per kg per day), and HDT (high-dose DS–LC, 200 mg per kg per day), with six mice per group. The CON group received a basic diet, while the other groups were fed a high-fat diet (87.5% basic feed, 10% lard, 2% cholesterol, and 0.5% pig bile salt). DS–LC was dissolved in 1% carboxymethyl cellulose (CMC), and both the CON and MC groups received an equivalent volume of 1% CMC *via* oral gavage. All groups were orally gavaged once daily for 28 days, with continuous access to food and water.

### 2.10 Serum lipids detection

After the final administration, mouse weights were measured, blood was collected by eye enucleation, and serum was immediately centrifuged at 5000 rpm for 10 minutes. The supernatant was then stored at −80 °C for subsequent use. Total cholesterol (TC), triglycerides (TG), high-density lipoprotein cholesterol (HDL-C), and low-density lipoprotein cholesterol (LDL-C) levels were determined using assay kits. The atherogenic index (AI) was calculated using the Fridewaid formula.[19]

$$\mathrm{AI}(\%) = \frac{\text{LDL-C}}{\text{HDL-C}} \times 100 \quad (2)$$

### 2.11 Organ index and histopathological detection

All mice were euthanized by cervical dislocation after blood collection, and the liver and epididymal adipose tissues were dissected. The organs were rinsed with physiological saline, blotted dry, and weighed. The liver and epididymal adipose tissue indices were calculated as a percentage of organ weight to body weight using formula (3).

$$\text{organ index}(\%) = \frac{\text{organ weight}}{\text{body weight}} \times 100 \quad (3)$$

The organ samples were initially rinsed with chilled saline to remove bloodstains, then fixed in 10% formalin for 48 hours and stored in 37 °C incubators for proper preservation. After stabilization in neutral formaldehyde solution, the samples were dehydrated, embedded in paraffin, and sectioned into 5 μm slices. These sections were then stained with hematoxylin-eosin (HE) for histological analysis. The histopathological changes were meticulously examined using a light microscope (BX53, Olympus, Japan) to evaluate tissue morphology and integrity.

### 2.12 Statistical analysis

The data are presented as means ± standard deviation (S.D.). Statistical analysis was conducted using SPSS 22.0 statistical software (IBM Corp, USA) through one-way analysis of variance (ANOVA), followed by the Least Significant Difference test (LSD) for homogeneous variances or the Dunnett's T3 test for non-homogeneous variances. A significance level of $p < 0.05$ was considered statistically significant.

## 3 Results and discussion

### 3.1 Analysis of DFR based on optimization of lecithin and daucosterol ratios

The DFR was determined by measuring the residual daucosterol through HPLC peak area analysis after the complexation reaction. Linear regression equations were used to calculate daucosterol concentrations in samples with different lecithin/daucosterol ratios, as shown in Fig. 1. A significant linear correlation was observed between daucosterol concentration and peak area, with the equation $y = 599\,198.28x - 554\,227$, where $y$ represents peak area and $x$ represents daucosterol concentration. When the lecithin/daucosterol ratio was 1 : 1, the DFR, calculated using formula (1), was 96.61%. For ratios of 2 : 1 and 3 : 1, their DFR exceeded 99%, reaching 99.74% and 99.62%, respectively. Based on these findings, a lecithin/daucosterol ratio of 2 : 1 was identified as optimal, maintaining high complexation efficiency while minimizing input.

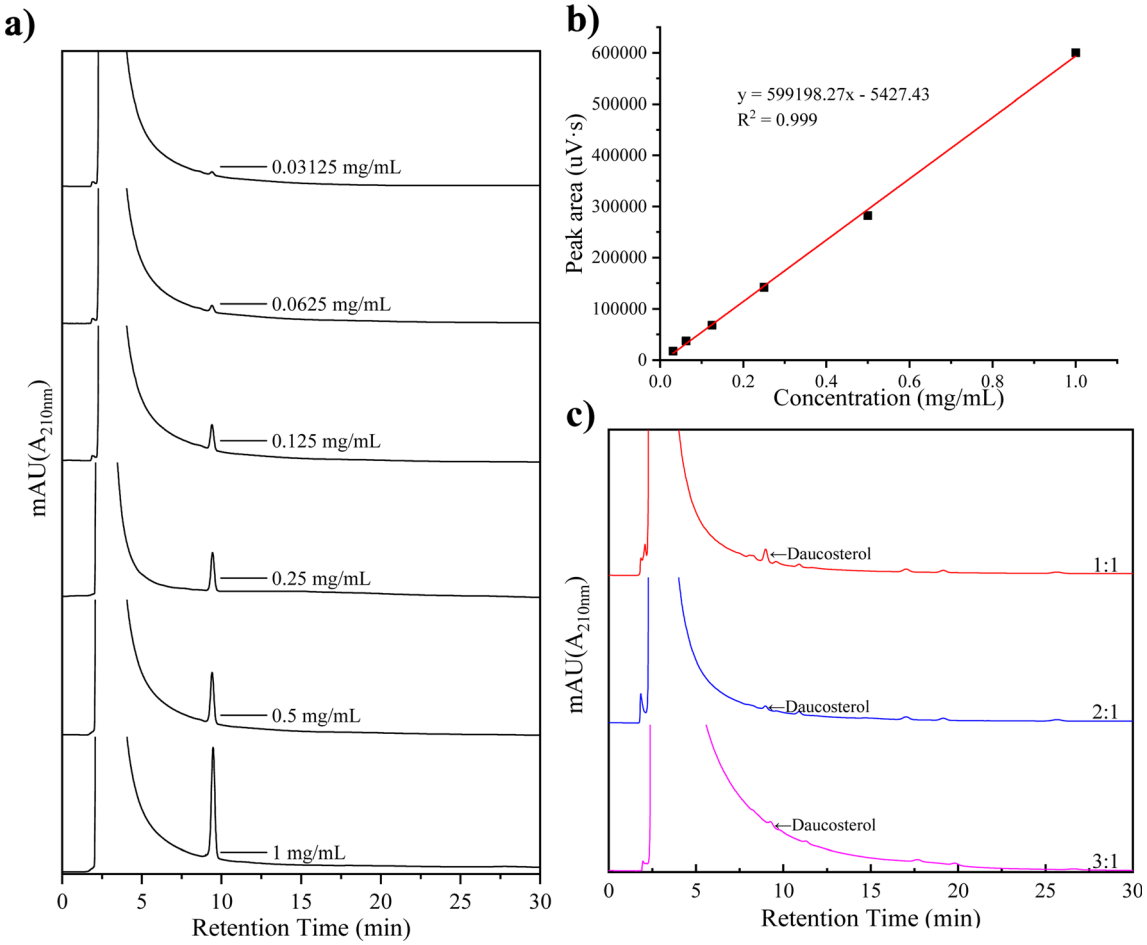


Fig. 1 Liquid chromatography spectra of daucosterol at various concentrations (a), standard curve (b), and chromatogram of incompletely complexed daucosterol (c).

### 3.2 Analysis of visual appearance and microstructure characteristics of DS–LC

The differences in appearance were observed among lecithin, daucosterol, their physical mixture, and DS–LC, as shown in Fig. 2. Lecithin appeared as light yellow, solid powder particles, while daucosterol was a dry white powder. When lecithin and daucosterol were physically mixed, the separate powders transformed into a sticky goose-yellow solid, with a lighter hue than pure lecithin. The DS–LC, however, presented a translucent beige color, lighter than both lecithin and the physical mixture, and displayed a state of aggregation, indicating greater homogeneity compared to the physical mixture. This homogeneity was pivotal for enhancing the bioavailability and stability of drugs encapsulated within the complex.[20] The change in appearance suggested that the aggregation formation of stable complexes between lecithin and daucosterol.

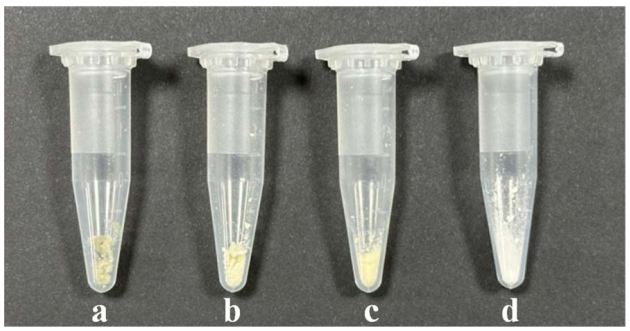


Fig. 2 Visual appearance of DS–LC (a), the physical mixture (b), lecithin (c) and daucosterol (d).

The microstructure characteristics, observed through SEM and depicted in Fig. 3, revealed that daucosterol exhibited a granular crystalline structure, while lecithin had irregular and dispersed surfaces without a uniform crystalline form. In the physical mixture, lecithin and daucosterol coexisted without altering their original morphologies. However, the DS–LC showed a structural transformation in daucosterol, which adopted an irregular form post-complexation. This change suggests an interaction between the crystalline structure of daucosterol and lecithin, leading to the integration of daucosterol within the lecithin matrix. The SEM images provided visual evidence of daucosterol's crystalline nature and lecithin's irregular morphology. While the physical mixture preserved the individual structures, the complexation process in DS–LC

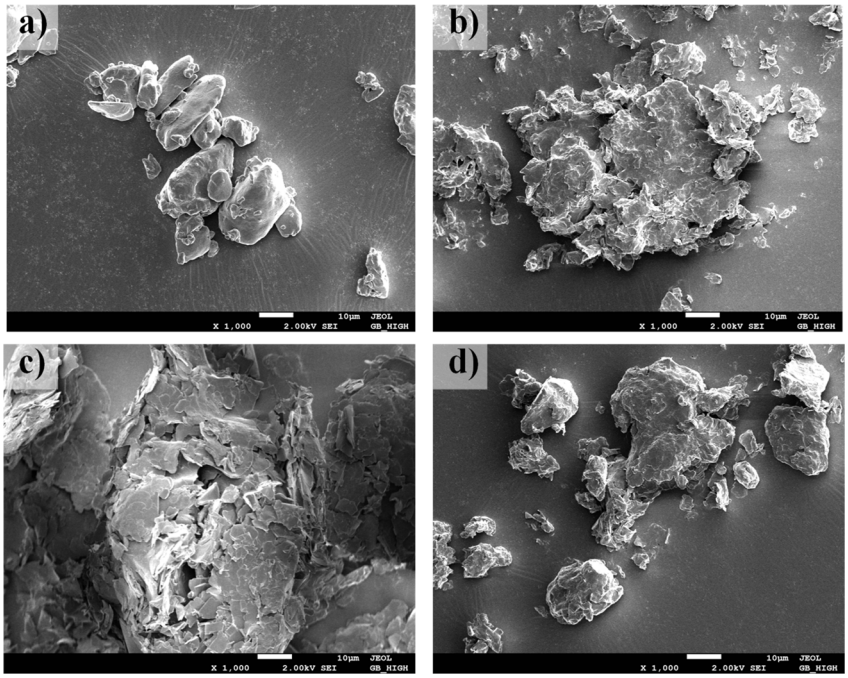


Fig. 3 Scanning electron micrographs of lecithin (a), daucosterol (b), the physical mixture (c) and DS–LC (d).

induced a structural alteration in daucosterol, indicating a robust interaction that integrates daucosterol into the lecithin matrix in an irregular form.

### 3.3 Analysis of molecular features of DS–LC by UV-vis and FTIR

The UV-vis spectra of DS–LC and daucosterol, shown in Fig. 4, both exhibit a peak at 210 nm, indicating that the chromophore structure of daucosterol remains intact within the DS–LC. This result suggests that the complexation process does not alter the chromophore structure,[21] preserving the molecular framework of daucosterol. The similarity in the UV-vis spectra between DS–LC and daucosterol confirmed that no new compound was formed during the complexation, highlighting the effectiveness of the process in maintaining the essential molecular features of daucosterol with minimal chemical changes. Further, The FTIR spectra, shown in Fig. 5, revealed that the infrared spectrum of the physical mixture closely resembled a combination of the individual spectra, with only minor shifts in intensity and wavenumber, indicating no chemical interactions during simple physical mixing. The characteristic peaks of lecithin, including the C=O stretching vibration at 1737 $cm^{-1}$ and the CH stretching of saturated long-chain fatty acids at 2924 $cm^{-1}$ and 2853 $cm^{-1}$, remained unchanged in both the physical mixture and DS–LC, suggesting that these functional groups did not participate in DS–LC formation. However, a significant shift in the OH stretching vibration peak to 3359 $cm^{-1}$ in the DS–LC spectrum indicated the formation of hydrogen bonds within the complex. It is well established that FTIR spectroscopy reliably detects such intermolecular interactions, as alterations in vibrational modes occur when hydrogen bonds form between acceptor and donor components.[22] Additionally, the increased intensity at 800 $cm^{-1}$ indicated molecular association between lecithin and daucosterol, enhancing the infrared absorption peak intensity. These findings imply the preservation of key molecular characteristics amidst the occurrence of specific intermolecular interactions during DS–LC complexation.

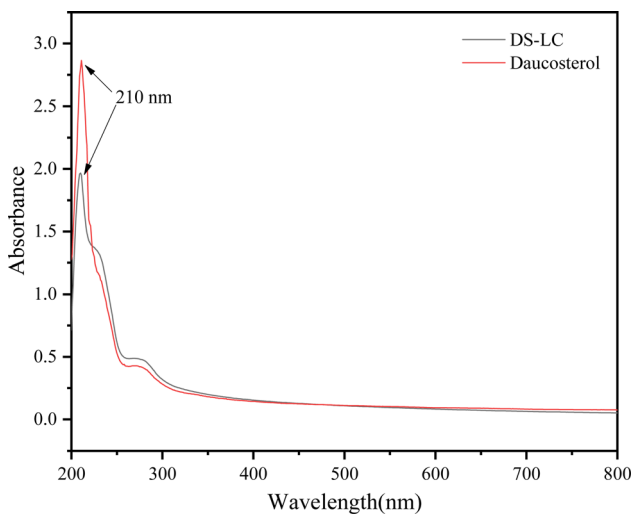


Fig. 4 UV-vis spectra of DS–LC and daucosterol.

### 3.4 Analysis of crystal structure of DS–LC by XRD

The XRD pattern shown in Fig. 6 revealed the distinct characteristics of daucosterol, lecithin, their physical mixture, and DS–LC. Daucosterol displayed clear crystalline peaks, confirming its crystalline nature, whereas lecithin appeared amorphous with no observable crystalline peaks. In the physical mixture, the

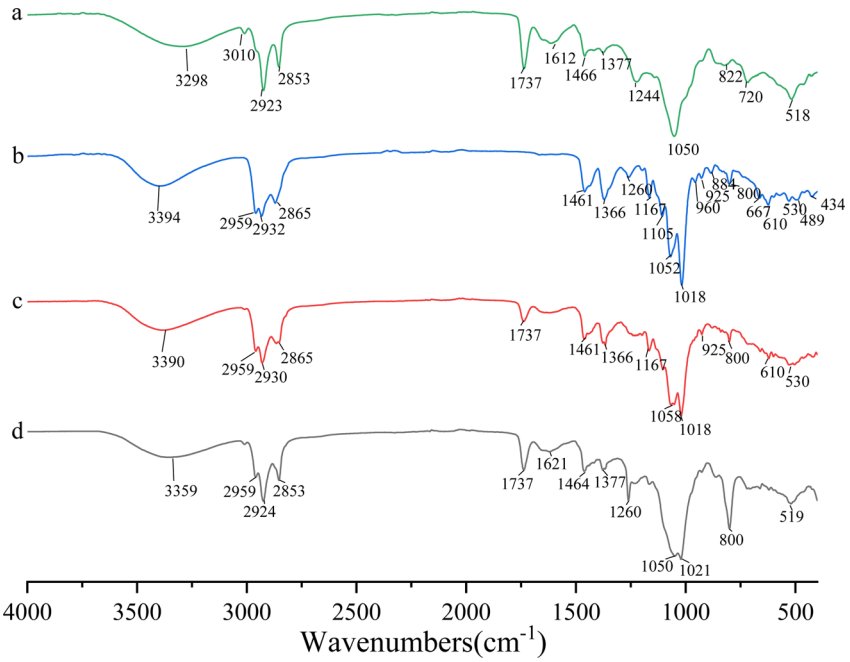


Fig. 5 Infrared spectra of lecithin (a), daucosterol (b), the physical mixture (c) and DS–LC (d).

crystalline peaks of daucosterol remained unchanged, indicating no significant interaction between the components, which was consistent with the expectation that physical mixing alone would not alter their structures.[21] However, within the DS–LC complex, lecithin significantly altered the diffraction pattern of daucosterol, with crystalline peaks less visible and

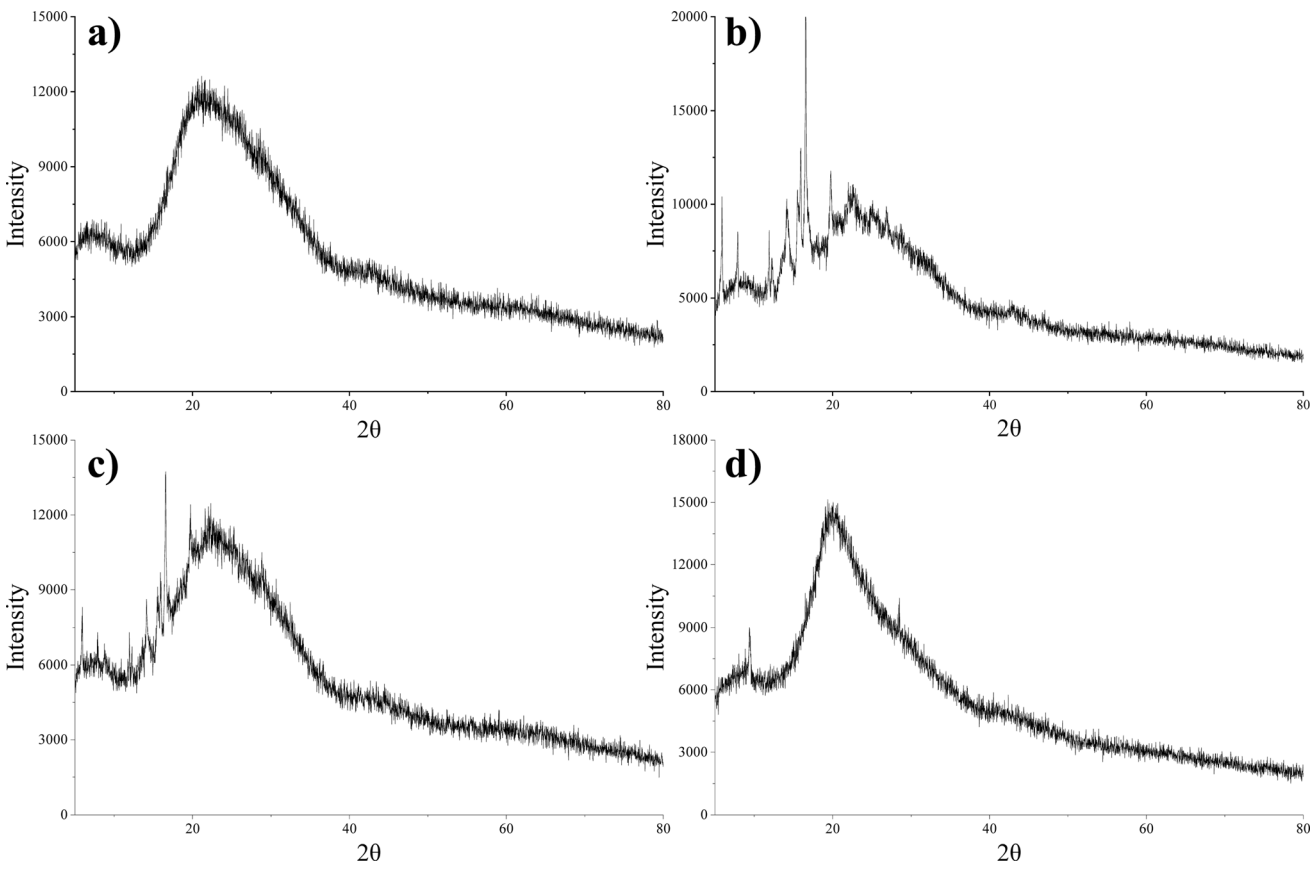


Fig. 6 X-ray diffraction patterns of lecithin (a), daucosterol (b), the physical mixture (c) and DS–LC (d).

some obscured by lecithin, indicating strong interaction between them. The complete disappearance of characteristic peaks in the DS–LC provided further evidence of this interaction, likely forming a new phase within the complex. These results indicated that daucosterol was uniformly distributed within the lecithin matrix in an irregular form. The interaction between the polar bonds of the two compounds likely played a crucial role in defining the structural characteristics of the DS–LC complex.

### 3.5 Analysis of thermal characteristics of DS–LC by DSC

The DSC peaks were analyzed to assess the formation of the complex. The DSC thermograms shown in Fig. 7 illustrated the thermal behavior of lecithin, daucosterol, their physical mixture, and DS–LC. Daucosterol displayed a distinct endothermic peak at approximately 312 °C. In contrast, the endothermic peak of daucosterol was absent in the DS–LC complex, replaced by a new peak around 286 °C. This shift suggested the formation of a novel phase transition peak,[23] likely due to the complexation between lecithin and daucosterol. The alteration in peak characteristics may be attributed to lecithin masking the distinctive features of daucosterol during complexation. Furthermore, the disappearance of daucosterol endothermic peak indicated a lack of crystalline structure and suggested that daucosterol was present in an irregular form within the complex. These results implied a homogeneous distribution of daucosterol within the lecithin matrix, indicating complex formation through intermolecular interactions.

### 3.6 Protective effect of DS–LC on liver and epididymal adipose tissue in hyperlipidemic mice

The liver and epididymal fat indices of mice in each group were presented in Table 1. The liver index in the MC group was significantly higher compared to the CON group ($p < 0.05$), with no significant difference between the MC and LDT groups ($p > 0.05$). Prolonged exposure to a high-fat diet generally stimulated hepatic *de novo* lipogenesis, exacerbating liver fat accumulation over time.[24] However, the liver index in the HDT group was significantly lower than in the MC group ($p < 0.05$). Similarly, the epididymal fat index was significantly higher in the MC group than in the CON group ($p < 0.05$), with no significant difference between the LDT and MC groups ($p > 0.05$). Notably, the epididymal fat index in the HDT group was significantly reduced compared to the MC group ($p < 0.05$). These results suggested that DS–LC may have exerted a protective effect on the liver and reduced epididymal fat accumulation in hyperlipidemic mice.

Table 1 The effect of DS–LC on organ index of mice ($n = 6$)[a]

| | The index of organs (%) | |
|---|---|---|
| Group | Liver | Epididymal adipose tissue |
| CON | $3.55 \pm 0.34^{b}$ | $1.32 \pm 0.53^{b}$ |
| MC | $4.20 \pm 0.40^{a}$ | $2.15 \pm 0.57^{a}$ |
| LDT | $3.82 \pm 0.41^{ab}$ | $1.76 \pm 0.46^{ab}$ |
| HDT | $3.67 \pm 0.40^{b}$ | $1.19 \pm 0.85^{b}$ |

[a] Different letters on values denote statistical significance ($p < 0.05$).

The morphology of liver and epididymal fat tissues, as shown in Fig. 8, revealed significant differences across groups. Mice in the CON group displayed healthy liver tissue with well-arranged cells, while those on a high-fat diet showed morphological changes such as cell swelling and steatosis. High-fat diet-induced liver lipid accumulation significantly damages the liver by promoting the production of toxic metabolites, resulting in hepatic inflammation and steatosis.[25,26] Treatment with DS–LC improved liver cell integrity and reduced fat accumulation. The LDT group showed fewer fat vesicles and less cell damage compared to the MC group, while the HDT group exhibited minimal fat vesicles or cell damage. Analysis of epididymal fat tissue revealed that fat cells were smaller in the CON group than in the MC group. Treatment with DS–LC reduced fat cell size, especially in the HDT group, where cells closely resembled those in the CON group. These findings demonstrated the effectiveness of DS–LC in reversing hepatic steatosis, enhancing liver health, and reducing lipid accumulation and fat cell size, with higher doses providing a more pronounced protective effect, indicating a potential positive impact on fat metabolism and liver health.

### 3.7 Regulation of serum TC, TG, and TC/TG levels by DS–LC in hyperlipidemic mice

TG constitute the primary component in adipose tissues, reflecting lipid accumulation, while TC encompasses the collective cholesterol content of serum lipoproteins.[27] The serum levels of TC, TG, and the TC/TG ratio in hyperlipidemic mice are presented in Fig. 9. Compared to the CON group, the MC model group showed a significant increase in both TC and TG levels ($p < 0.05$). Following DS–LC treatment, both the LDT

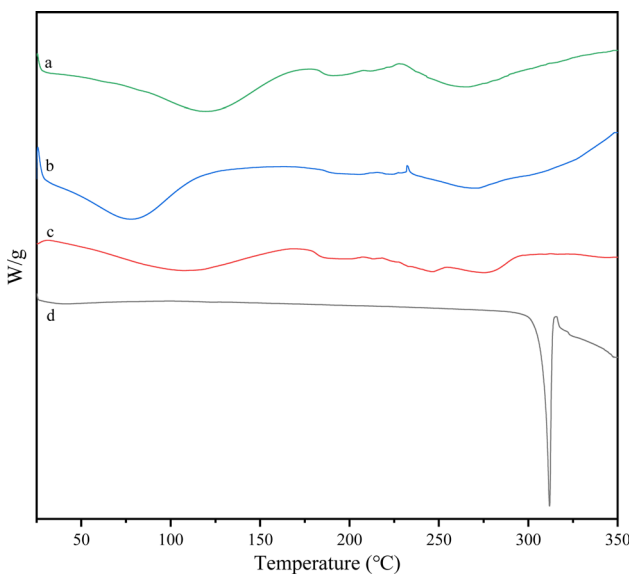


Fig. 7 Differential scanning calorimetry curves of lecithin (a), the physical mixture (b), DS–LC (c) and daucosterol (d).

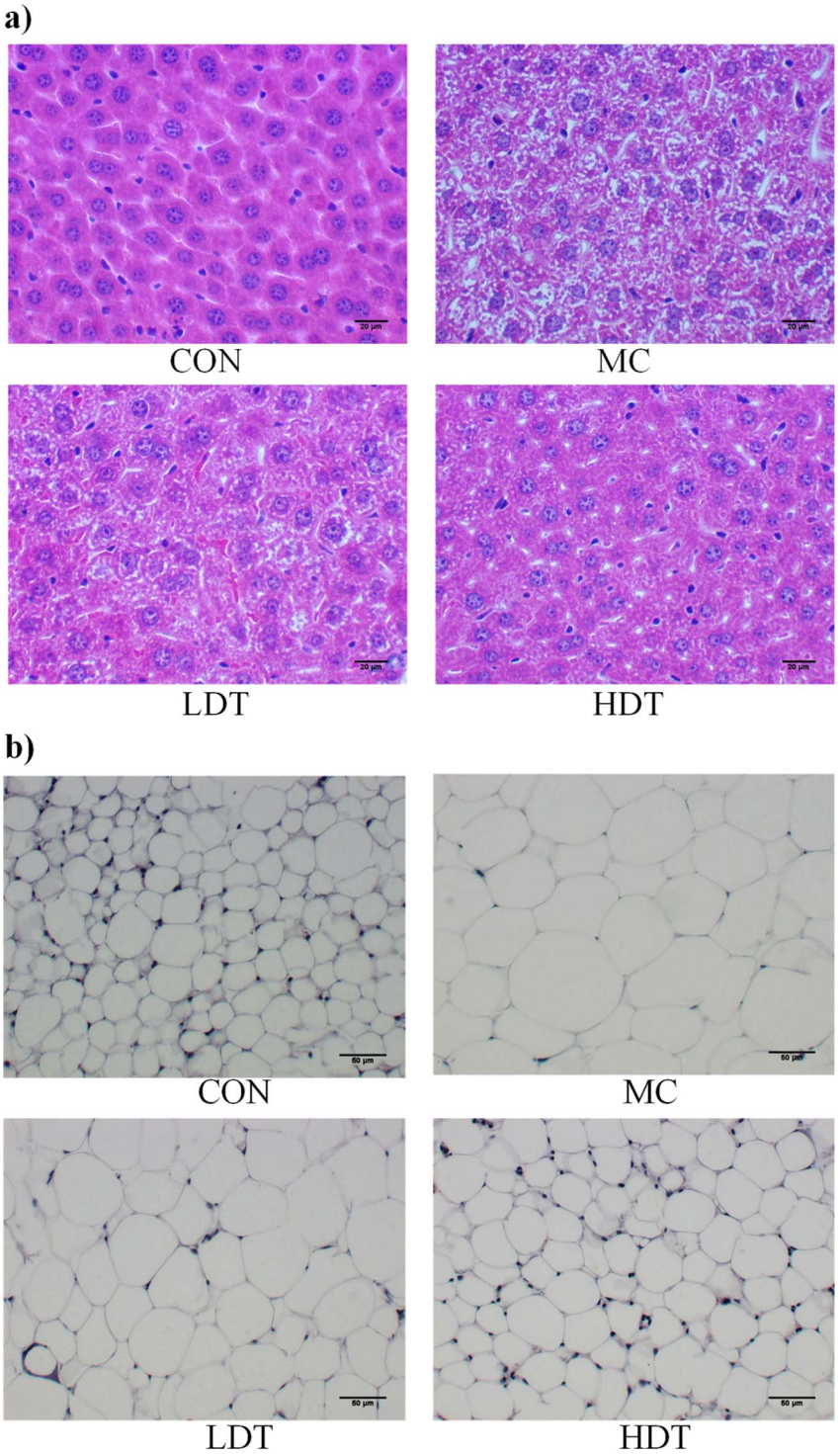


Fig. 8 Histopathological images of liver tissue (a) and adipose tissue (b) near the epididymis in each group.

and HDT groups exhibited a significant reduction in TC levels compared to the MC group ($p < 0.05$). Additionally, the HDT group showed a significant decrease in TG levels ($p < 0.05$), whereas the reduction in the LDT group was not statistically significant ($p > 0.05$). The MC group had a significantly lower TC/TG ratio compared to the CON group. After DS–LC administration, both the LDT and HDT groups showed an increase in this ratio, with the most pronounced rise observed in the HDT group ($p < 0.05$). These results indicated that a higher dose of DS–LC had a more substantial lipid-lowering effect than a lower dose. DS–LC appeared to exert a hypolipidemic effect by lowering serum TC and TG levels, thereby aiding in the management of dyslipidemia.

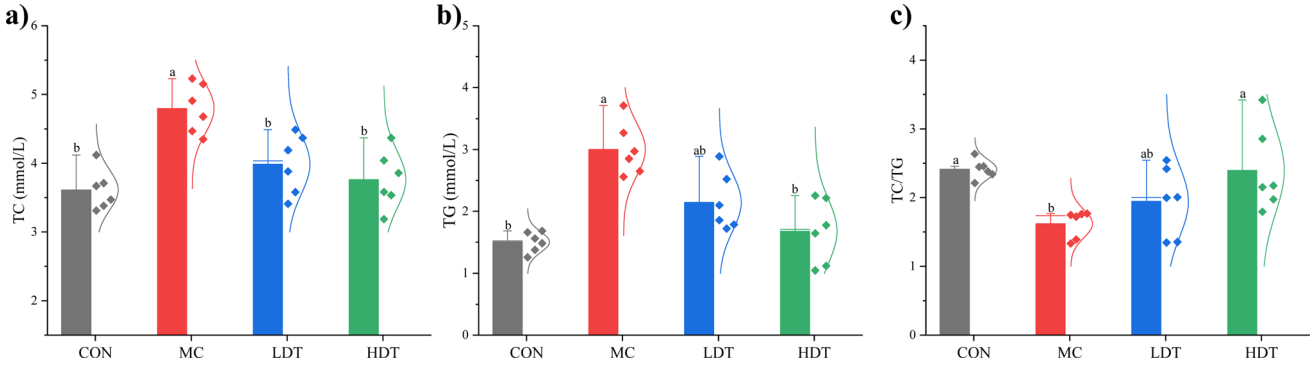


Fig. 9 The serum levels of TC (a), TG (b), and the TC/TG ratio (c) of mice in each group.

Table 2 The effect of DS–LC on HDL-C, LDL-C and AI of mice ($n = 6$)[a]

| Group | HDL-C | LDL-C | AI (%) |
|---|---|---|---|
| CON | 1.68 ± 0.08 | 1.03 ± 0.04[b] | 0.62 ± 0.03[b] |
| MC | 1.41 ± 0.10 | 1.85 ± 0.19[a] | 1.34 ± 0.14[a] |
| LDT | 1.46 ± 0.20 | 1.64 ± 0.17[a] | 1.13 ± 0.20[a] |
| HDT | 1.52 ± 0.12 | 0.92 ± 0.15[b] | 0.61 ± 0.10[b] |

[a] Different letters on values denote statistical significance ($p < 0.05$).

### 3.8 Regulation of serum HDL-C, LDL-C and AI levels by DS–LC in hyperlipidemic mice

LDL-C and HDL-C play crucial roles in transporting endogenous cholesterol within the liver. LDL-C, prone to oxidation, promotes atherosclerosis by forming cholesterol-rich foam, while HDL-C prevents LDL-C oxidation, impedes cholesterol transportation to the liver, and protects cardiovascular health.[27,28] The serum levels of HDL-C, LDL-C, and AI in hyperlipidemic mice were presented in Table 2. Across various groups, no statistically significant differences were observed in HDL-C levels ($p > 0.05$). However, DS–LC administration effectively reduced serum LDL-C levels, particularly in the high-dose DS–LC (HDT) group, where a significant decrease in LDL-C was noted compared to the model control (MC) group ($p < 0.05$). Additionally, the AI showed a significant reduction in both the LDT and HDT groups ($p < 0.05$). The arteriosclerosis index is a key indicator for assessing the risk of developing arteriosclerosis, with LDL-C accumulation in blood vessels being a major contributing factor.[29,30] These findings suggested that DS–LC might help reduce the risk of arteriosclerosis by lowering LDL-C levels, indicating its potential as a therapeutic agent for managing cholesterol-related conditions.

## 4 Conclusions

The preparation of DS–LC involved the utilization of daucosterol from *Eleocharis dulcis* and lecithin through the solvent evaporation technique. A comprehensive analysis was conducted to characterize DS–LC and assess its impact on lipid metabolism in hyperlipidemic mice. Firstly, DS–LC effectively formed a complex with lecithin, achieving high complexation rates, particularly at a lecithin/daucosterol ratio of 2 : 1. This ratio provided an optimal balance between complexation efficiency and minimal input. Visual appearance analysis revealed that DS–LC appeared as a translucent beige and exhibited aggregation, differing from the physical appearance of lecithin, daucosterol, and their physical mixture. UV-vis spectra confirmed that DS–LC and daucosterol shared a common chromophore structure, indicating that daucosterol's molecular framework was preserved within the complex. Infrared spectroscopy analysis indicated molecular interactions during DS–LC formation, with the emergence of hydrogen bonds and increased peak intensity. XRD and SEM analyses further confirmed the formation of DS–LC, indicating the integration of daucosterol into the lecithin matrix in an irregular pattern. Crucially, DS–LC treatment yielded positive results in hyperlipidemic mice, including improved liver health, reduced lipid accumulation, and modulation of serum lipid levels. Notably, this treatment led to a reduction in LDL-C levels, a vital factor in decreasing the likelihood of arteriosclerosis. These findings underscore the potential therapeutic advantages of DS–LC for managing lipid metabolism and its significance as a treatment for cholesterol-related disorders.

## Ethical statement

All mice used in this study were obtained from the Guangdong Medical Experimental Animal Center (Guangdong, China), kept in a pathogen-free environment, and fed ad libitum. All procedures were conducted in accordance with the 'Guiding Principles in the Care and Use of Animals' (China) and approved by the Ethics Committee of the Guangdong Provincial Department of Science and Technology (Laboratory Animal Use License Number: SYXK [Yue] 20190204). The study strictly adhered to the 'Regulations on the Administration of Laboratory Animals' issued by the Ministry of Science and Technology of the People's Republic of China.

## Data availability

The authors confirm that the data supporting the findings of this study are available within the article. The raw data that support the findings of this study are available from the corresponding author, upon reasonable request.

## Author contributions

Conceptualization, Yipeng Gu and Xiaomei Yang; data curation, Dingjin Li; formal analysis, Liang Shuai and Dingjin Li; investigation, Yipeng Gu and Xiaomei Yang; methodology, Yipeng Gu; software and visualization, Mobo Song and Yingjian Liu; validation, Yipeng Gu and Liang Shuai; writing – original draft, Yipeng Gu; writing – review & editing, Xiaomei Yang.

## Conflicts of interest

The authors have declared no conflicts of interest.

## Acknowledgements

This study received support from the Guangxi Science and Technology Base and Talent Special Project (Guike AD23026036), the Annual University-Level Research Projects of Hezhou University (2023BSQD08) and Guangxi University Student Innovation and Entrepreneurship Training Program Project (S202411838022). The authors sincerely appreciate the material and technical support from Guangxi First-Class Discipline (Food Science and Engineering), the Guangxi Education System's Outstanding Teachers Study Abroad and Further Education Program in 2023 (Guijiaoshipei [2023] No. 13), and the Guangxi Key Research and Development Project (Guike AB23049007). Special thanks to Liu Xinxin for his valuable guidance in animal model development.

## References

1 K.-X. Zhang, Y. Zhu, S.-X. Song, Q.-Y. Bu, X.-Y. You, H. Zou and G.-P. Zhao, Ginsenoside Rb1, Compound K and 20(S)-Protopanaxadiol Attenuate High-Fat Diet-Induced Hyperlipidemia in Rats via Modulation of Gut Microbiota and Bile Acid Metabolism, *Molecules*, 2024, **29**, 1108, DOI: **10.3390/molecules29051108**.

2 D. Georgia-Eirini, S. Athina, V. B. Wim, K. Christos and C. Theodoros, Natural Products from Mediterranean Diet: From Anti-Hyperlipidemic Agents to Dietary Epigenetic Modulators, *Curr. Pharm. Biotechnol.*, 2019, **20**, 825–844, DOI: **10.2174/1573407215666190628150921**.

3 R. Sreedhar, V. S. Kumar, A. K. Bhaskaran Pillai and S. Mangalathillam, Omega-3 Fatty Acid Based Nanolipid Formulation of Atorvastatin for Treating Hyperlipidemia, *Adv. Pharm. Bull.*, 2019, **9**, 271–280, DOI: **10.15171/apb.2019.031**.

4 H. Wu, Z. Yu and Q. Huang, Characteristics of Serum Lipid Levels in Patients with Hypertension: A Hospital-Based Retrospective Descriptive Study, *BMJ Open*, 2022, **12**, e054682, DOI: **10.1136/bmjopen-2021-054682**.

5 A. Kumari, K. K. Kristensen, M. Ploug and A.-M. L. Winther, The Importance of Lipoprotein Lipase Regulation in Atherosclerosis, *Biomedicines*, 2021, **9**, 782, DOI: **10.3390/biomedicines9070782**.

6 B. A. Ference, H. N. Ginsberg, I. Graham, K. K. Ray, C. J. Packard, E. Bruckert, R. A. Hegele, R. M. Krauss, F. J. Raal, H. Schunkert, *et al.*, Low-Density Lipoproteins Cause Atherosclerotic Cardiovascular Disease. 1. Evidence from Genetic, Epidemiologic, and Clinical Studies. A Consensus Statement from the European Atherosclerosis Society Consensus Panel, *Eur. Heart J.*, 2017, **38**, 2459–2472, DOI: **10.1093/eurheartj/ehx144**.

7 Y. E. Park, M. S. Kim, K. W. Shim, Y.-I. Kim, J. Chu, B.-K. Kim, I. S. Choi and J. Y. Kim, Effects of Lactobacillus Plantarum Q180 on Postprandial Lipid Levels and Intestinal Environment: A Double-Blind, Randomized, Placebo-Controlled, Parallel Trial, *Nutrients*, 2020, **12**, 255, DOI: **10.3390/nu12010255**.

8 B. Lee, K. Han, H.-J. Park, A.-R. Kim, O.-J. Kwon, C. Yang and C.-S. Cho, Efficacy of Hwangryunhaedok-Tang (Huang-Lian-Jie-Du-Tang, Oren-Gedoku-to) for Patients with Hyperlipidemia: A Study Protocol for a Randomized, Double-Blind, Placebo-Controlled, Parallel, Investigator-Initiated Clinical Trial, *Trials*, 2020, **21**, 750, DOI: **10.1186/s13063-020-04695-3**.

9 J. Li, S. Wang, B. Wang, H. Wei, X. Liu, J. Hao, Y. Duan, J. Hua, X. Zheng, X. Feng, *et al.*, High-Fat-Diet Impaired Mitochondrial Function of Cumulus Cells but Improved the Efficiency of Parthenogenetic Embryonic Quality in Mice, *Anim. Cells Syst.*, 2018, **22**, 243–252, DOI: **10.1080/19768354.2018.1497707**.

10 H. C. Nguyen, M. Qadura and K. K. Singh, Role of the Fatty Acid Binding Proteins in Cardiovascular Diseases: A Systematic Review, *J. Clin. Med.*, 2020, **9**, 3390, DOI: **10.3390/jcm9113390**.

11 S. Kathiresan and D. Srivastava, Genetics of Human Cardiovascular Disease, *Cell*, 2012, **148**, 1242–1257, DOI: **10.1016/j.cell.2012.03.001**.

12 N. El Omari, I. Jaouadi, M. Lahyaoui, T. Benali, D. Taha, S. Bakrim, N. El Menyiy, F. El Kamari, G. Zengin, S. P. Bangar, *et al.*, Natural Sources, Pharmacological Properties, and Health Benefits of Daucosterol: Versatility of Actions, *Appl. Sci.*, 2022, **12**, 5779, DOI: **10.3390/app12125779**.

13 X. Yang, Y. Gu, H. Liu, F. Shang and T. Koyama, Modulation of the Gut Microbiota Alleviates Insulin Resistance in Type 2 Diabetic Mice by Daucosterol from *Eleocharis Dulcis* Peel, *J. Funct. Foods*, 2024, **114**, 106092, DOI: **10.1016/j.jff.2024.106092**.

14 V. Jain, S. K. Verma and S. S. Katewa, Therapeutic Validation of Ipomoea Digitata Tuber (Ksheervidari) for Its Effect on Cardio-Vascular Risk Parameters, *Indian J. Tradit. Knowl.*, 2011, **10**, 617–623.

15 V. N. Mironova and L. A. Kalashnikova, Hypolipidemic Action of Beta-D-Glycoside Beta-Sitosterol in the Rat, *Farmakol. Toksikol.*, 1982, **45**, 45–47.

16 X. Zhao, C. Shi, X. Zhou, T. Lin, Y. Gong, M. Yin, L. Fan, W. Wang and J. Fang, Preparation of a Nanoscale Dihydromyricetin-Phospholipid Complex to Improve the Bioavailability: In Vitro and in Vivo Evaluations, *Eur. J. Pharm. Sci.*, 2019, **138**, 104994, DOI: **10.1016/j.ejps.2019.104994**.

17 Z. Song, J. Yin, P. Xiao, J. Chen, J. Gou, Y. Wang, Y. Zhang, T. Yin, X. Tang and H. He, Improving Breviscapine Oral Bioavailability by Preparing Nanosuspensions, Liposomes and Phospholipid Complexes, *Pharmaceutics*, 2021, **13**, 132, DOI: **10.3390/pharmaceutics13020132**.

18 Y. Gu, X. Yang, C. Shang, T. T. P. Thao and T. Koyama, Inhibitory Properties of Saponin from *Eleocharis Dulcis* Peel against α-Glucosidase, *RSC Adv.*, 2021, **11**, 15400–15409, DOI: **10.1039/D1RA02198B**.

19 S. Du, Y. Lv, N. Li, X. Huang, X. Liu, H. Li, C. Wang and Y.-F. Jia, Biological Investigations on Therapeutic Effect of Chitosan Encapsulated Nano Resveratrol against Gestational Diabetes Mellitus Rats Induced by Streptozotocin, *Drug Delivery*, 2020, **27**, 953–963, DOI: **10.1080/10717544.2020.1775722**.

20 K. Kuche, N. Bhargavi, C. P. Dora and S. Jain, Drug-Phospholipid Complex—a Go through Strategy for Enhanced Oral Bioavailability, *AAPS PharmSciTech*, 2019, **20**, 43.

21 K. Brad and Y. Zhang, Study on Extraction and Purification of Apigenin and the Physical and Chemical Properties of Its Complex with Lecithin, *Pharmacogn. Mag.*, 2018, **14**, 203.

22 A. Shayganpour, S. Naderizadeh, S. Grasselli, A. Malchiodi and I. S. Bayer, Stacked-Cup Carbon Nanotube Flexible Paper Based on Soy Lecithin and Natural Rubber, *Nanomaterials*, 2019, **9**, 824, DOI: **10.3390/nano9060824**.

23 Y. Zhang, Q. Li, J. Hu, C. Wang, D. Wan, Q. Li, Q. Jiang, L. Du and Y. Jin, Nasal Delivery of Cinnarizine Thermo-and Ion-Sensitive in Situ Hydrogels for Treatment of Microwave-Induced Brain Injury, *Gels*, 2022, **8**, 108.

24 Y. Paalvast, A. Gerding, Y. Wang, V. W. Bloks, T. H. Van Dijk, R. Havinga, K. Willems Van Dijk, P. C. N. Rensen, B. M. Bakker, J. A. Kuivenhoven, *et al.*, Male apoE*3-Leiden.CETP Mice on High-Fat High-Cholesterol Diet Exhibit a Biphasic Dyslipidemic Response, Mimicking the Changes in Plasma Lipids Observed through Life in Men, *Physiol. Rep.*, 2017, **5**, e13376, DOI: **10.14814/phy2.13376**.

25 L. Crudele, C. De Matteis, E. Piccinin, R. M. Gadaleta, M. Cariello, E. Di Buduo, G. Piazzolla, P. Suppressa, E. Berardi, C. Sabbà, *et al.*, Low HDL-Cholesterol Levels Predict Hepatocellular Carcinoma Development in Individuals with Liver Fibrosis, *JHEP Rep.*, 2023, **5**, 100627, DOI: **10.1016/j.jhepr.2022.100627**.

26 Q. He, Y. Diao, T. Zhao, B. Hou, L. D. Ngokana, H. Liang, J. Nie, P. Tan, H. Huang, Y. Li, *et al.*, SREBP1c Mediates the Effect of Acetaldehyde on Cidea Expression in Alcoholic Fatty Liver Mice, *Sci. Rep.*, 2018, **8**, 1200, DOI: **10.1038/s41598-018-19466-z**.

27 S. Ruan, X. Gao, B. Li and J. Tian, The Synergic Effects and Mechanism of KGM–DMY Complex in the Prevention of Obesity and Enhancement of Fatigue Resistance in Mice, *Food Funct.*, 2023, **14**, 2607–2620.

28 L. J. Goldstein and S. M. Brown, The Low-Density Lipoprotein Pathway and Its Relation to Atherosclerosis, *Annu. Rev. Biochem.*, 1977, **46**, 897–930, DOI: **10.1146/annurev.bi.46.070177.004341**.

29 J. Hu, M. Liu, R. Yang, L. Wang, L. Liang, Y. Yang, S. Jia, R. Chen, Q. Liu, Y. Ren, *et al.*, Effects of High-Intensity Interval Training on Improving Arterial Stiffness in Chinese Female University Students with Normal Weight Obese: A Pilot Randomized Controlled Trial, *J. Transl. Med.*, 2022, **20**, 60, DOI: **10.1186/s12967-022-03250-9**.

30 S. H. Aladaileh, S. A. M. Saghir, K. Murugesu, A. Sadikun, A. Ahmad, G. Kaur, A. M. Mahmoud and V. Murugaiyah, Antihyperlipidemic and Antioxidant Effects of Averrhoa Carambola Extract in High-Fat Diet-Fed Rats, *Biomedicines*, 2019, **7**, 72, DOI: **10.3390/biomedicines7030072**.